

Automated Laser-Transfer Synthesis of High-Density Microarrays for Infectious Disease Screening

Grigori Paris, Jasmin Heidepriem, Alexandra Tsouka, Yuxin Liu, Daniela S. Mattes, Sandra Pinzón Martín, Pietro Dallabernardina, Marco Mende, Celina Lindner, Robert Wawrzinek, Christoph Rademacher, Peter H. Seeberger, Frank Breitling, Frank Ralf Bischoff, Timo Wolf, and Felix F. Loeffler*

Laser-induced forward transfer (LIFT) is a rapid laser-patterning technique for high-throughput combinatorial synthesis directly on glass slides. A lack of automation and precision limits LIFT applications to simple proof-of-concept syntheses of fewer than 100 compounds. Here, an automated synthesis instrument is reported that combines laser transfer and robotics for parallel synthesis in a microarray format with up to 10 000 individual reactions cm^{-2} . An optimized pipeline for amide bond formation is the basis for preparing complex peptide microarrays with thousands of different sequences in high yield with high reproducibility. The resulting peptide arrays are of higher quality than commercial peptide arrays. More than 4800 15-residue peptides resembling the entire Ebola virus proteome on a microarray are synthesized to study the antibody response of an Ebola virus infection survivor. Known and unknown epitopes that serve now as a basis for Ebola diagnostic development are identified. The versatility and precision of the synthesizer is demonstrated by in situ synthesis of fluorescent molecules via Schiff base reaction and multi-step patterning of precisely definable amounts of fluorophores. This automated laser transfer synthesis approach opens new avenues for high-throughput chemical synthesis and biological screening.


1. Introduction

Automated chemical synthesis reduced repetitive manual operations and revolutionized the discovery of functional compounds. Most sophisticated automated synthesis instruments are optimized to perform successive iterations of robust reactions for a single compound class: The well-defined and iterative character of peptide and oligonucleotide syntheses led to the development of automated solid-phase synthesis strategies that provide quick access to oligomers.^[1,2] Inspired by these approaches, the automated synthesis of oligosaccharides^[3] has significantly progressed and recently, the concept was adapted to the synthesis of small molecules.^[4] The latter automated synthesis approaches focus on the generation of a single target molecule at a time. Proteome-wide epitope screening that requires the synthesis of thousands of peptides, cannot

G. Paris, J. Heidepriem, A. Tsouka, Y. Liu, S. Pinzón Martín, P. Dallabernardina, M. Mende, C. Lindner, R. Wawrzinek, P. H. Seeberger, F. F. Loeffler
Department of Biomolecular Systems
Max Planck Institute of Colloids and Interfaces
Am Muehlenberg 1, 14476 Potsdam, Germany
E-mail: Felix.Loeffler@mpikg.mpg.de

G. Paris
Department of System Dynamics and Friction Physics
Institute of Mechanics
Technical University of Berlin
Str. des 17. Juni 135, 10623 Berlin, Germany

J. Heidepriem, A. Tsouka, Y. Liu, S. Pinzón Martín, P. H. Seeberger
Institute of Chemistry and Biochemistry
Freie Universität Berlin
Arnimallee 22, 14195 Berlin, Germany

 The ORCID identification number(s) for the author(s) of this article can be found under <https://doi.org/10.1002/adma.202200359>.

© 2022 The Authors. Advanced Materials published by Wiley-VCH GmbH. This is an open access article under the terms of the Creative Commons Attribution License, which permits use, distribution and reproduction in any medium, provided the original work is properly cited.

D. S. Mattes, F. Breitling
Institute of Microstructure Technology
Karlsruhe Institute of Technology
Hermann-von-Helmholtz-Platz 1, 76344 Eggenstein-Leopoldshafe, Germany

C. Rademacher
Department of Pharmaceutical Sciences
University of Vienna
Althanstr. 14, Vienna 1090, Austria

C. Rademacher
Department of Microbiology and Immunobiology
Max F. Perutz Laboratories GmbH
Dr.-Bohr-Gasse 9, Vienna 1030, Austria

F. R. Bischoff
Department of Functional Genome Analysis
German Cancer Research Center
Im Neuenheimer Feld 580, 69120 Heidelberg, Germany

T. Wolf
Infectious Diseases Unit
Department of Medicine
Goethe University Hospital
Theodor-Stern-Kai 7, 60590 Frankfurt am Main, Germany

DOI: 10.1002/adma.202200359

Table 1. Commercially established technologies for the synthesis of high-density peptide microarrays.

| | SPOT | Photolithographic | Particle-based | Laser-based (this work) |
|-----------------------------------|--|---------------------------------------|----------------------------|-------------------------|
| Synthesis approach | membrane, Fmoc-protection | glass, photo-labile protecting groups | glass, Fmoc-protection | glass, Fmoc-protection |
| Deposition procedure | syringe delivery | microfluidic delivery | xerography | laser transfer |
| Spot density [cm^{-2}] | up to 25 ^[18] | up to 22 000 ^[19] | up to 1250 ^[20] | up to 10 000 |
| Peptide length | up to 25 residues | up to 12 residues | up to 20 residues | up to 20 residues |
| Spot morphology | stable, coffee-ring | stable, ghost spots | stable, blurred | stable |
| Coupling yield | ≈95%, purification after cleavage possible | ≈75% ^[17] | ≈90% ^[10] | ≈95% |

be addressed with this approach. Parallel peptide production in an array format increases synthesis throughput and decreases the cost of goods. This high-throughput synthesis concept was introduced in the 1980s^[5] and since continues to evolve.^[6–16]

The SPOT,^[6] photolithographic,^[7] and particle-based^[10] syntheses are now commercialized^[18–20] and commonly used to prepare peptides for binding studies.^[21–23] However, each approach has at least one major drawback in regards to the peptide spot density, the possible peptide length, or the resulting peptide spot morphology (Table 1). To overcome these limitations, laser-induced forward transfer can be used for the in situ generation of high-density peptide microarrays: Different types of pre-activated polymer embedded amino acids are precisely

transferred by laser irradiation from easily exchangeable donor slides to a functionalized acceptor slide in a polymer spot pattern (Figure 1). Then, the resulting nanometer thin polymer spots, serving as “solid” solvent, allow for an on-demand heat-induced coupling reaction in parallel. Heated above the glass transition temperature of the polymer, in each spot, the specific pre-activated amino acid (AA) type reacts with the amino-functionalized acceptor slide. Consecutively, the acceptor slide can be washed (removal of excess AA and polymer), capped (acetylation of non-reacted amino groups on the surface), and deprotected, which enables coupling of subsequent AAs. By repeating the procedure, the in situ built-up of the desired peptide sequences in the array format is performed.

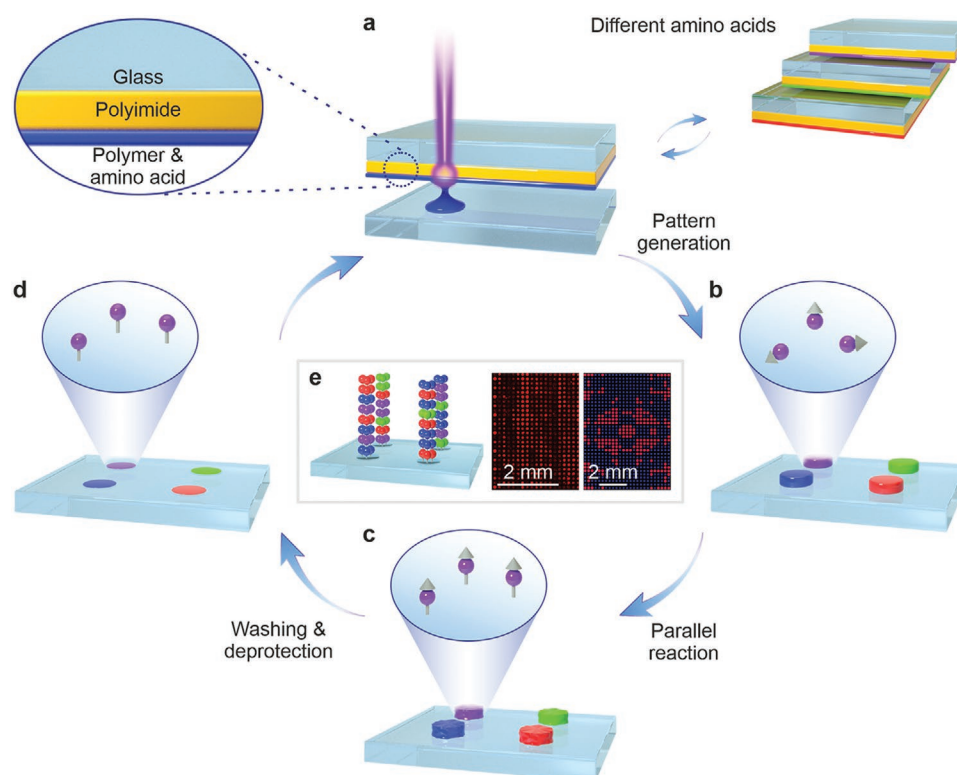


Figure 1. Principle of the laser-based peptide microarray synthesis. a) Material is transferred from different types of amino acid donor slides to a functionalized acceptor slide in a b) polymer reactor spot pattern. c) The polymer pattern is heated above the glass transition temperature allowing the pre-activated amino acids to couple to the amino-functionalized surface. d) Subsequently, the acceptor slide is washed, capped, and deprotected. e) Repeating the procedure enables the in situ synthesis of peptides in a microarray format.

Compared to liquid solvent-based in situ microarray synthesis approaches^[16,24] that require hydrophobic functionalization of the synthesis surface, the laser-based polymer transfer does not require this pre-treatment. Moreover, such technology is especially useful for rapidly generating individually customized arrays, which can aid diagnosis and monitoring of infectious^[25] or autoimmune diseases^[26] as rationally designed antigen variants can be quickly screened.

We described the principle previously,^[14] but until today the process was limited to simple array syntheses of up to 64 short (9-residue) peptides,^[14,27] due to insufficient robustness and reproducibility of the process. Recent progress in the theoretical and experimental understanding of the laser transfer mechanism helped to overcome these obstacles. Precise and reproducible patterning is now possible,^[28] while the laser process temperature can be adjusted for more demanding AAs.^[29]

Here, we report an automated laser-based synthesizer that produces arrays with a spot density of up to 10000 spots cm^{-2} . Combined with an optimization pipeline that can be adapted for various other in situ printing techniques, we are now able to synthesize complex microarrays containing thousands of different molecules in high yield and high reproducibility. The synthesis quality of this new methodology is superior as illustrated by comparing our peptide microarrays with a commercially available reference. The complete Ebola virus proteome was synthesized on a microarray with >4800 15-residue peptides to study the recognition of B cell epitopes in an Ebola virus disease survivor. Finally, we show the versatility and precision of the synthesizer by in situ synthesis of fluorescent molecules via Schiff base reaction and multi-step patterning of precisely definable amounts of fluorophores. This offers a new way for high-throughput chemical reaction screening in polymer reactors.

2. Results and Discussion

2.1. Automated Laser-Based High-Precision Synthesizer

The key characteristics of in situ generated peptide microarrays are the resulting spot density, spot morphology, and synthesis yield. These three features heavily rely on a precise and reproducible AA transfer. Therefore, we developed a microarray synthesizer (**Figure 2**; Figures S1–S3, Supporting Information) that utilizes our laser-based transfer approach with a reproducible and high transfer precision, automated by a robotic arm. A graphical user interface enables non-specialists to initiate the automated procedure. The synthesizer contains four expandable modules (Movie S1, Supporting Information): 1) Up to four acceptor and 23 different donor slides can be manually loaded into the slide holder. 2,3) A robot transports these slides between the slide holder and the positioning table, 4) while the laser system automatically transfers the AAs. An acceptor slide is reproducibly aligned on the positioning table by three positioning bolts. Then, different donor slides are placed successively on top of the acceptor slide and the laser transfer is performed. To prohibit local overheating of the donor slide material during the laser transfer process, we implemented

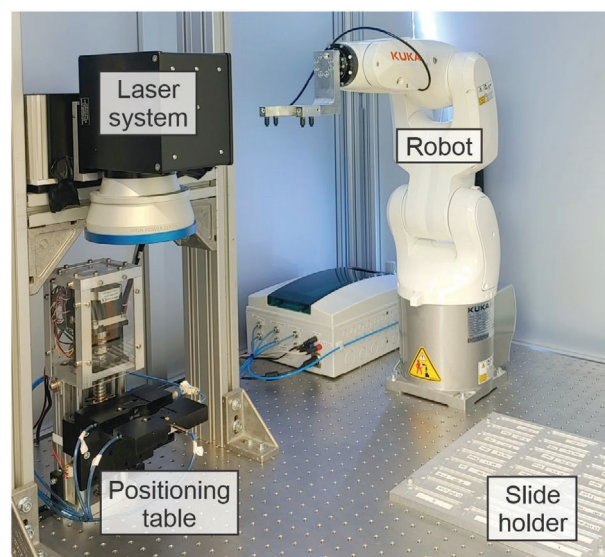


Figure 2. Automated laser-based microarray synthesizer. The system comprises: a slide holder for acceptor and donor slides; a robot with gripper tool for transportation of acceptor and donor slides; a positioning table with automated alignment of acceptor slides; a laser system with a 405 nm diode laser and laser scanning system.

a random spot transfer algorithm (Figure S4, Supporting Information).

2.2. Optimization of the Laser-Based In Situ Peptide Microarray Synthesis

Upon increasing the spot density, all in situ synthesis technologies eventually suffer from yield and spot morphology problems. Therefore, we developed an optimization pipeline for our laser-based in situ solid-phase peptide synthesis approach to optimize the transfer and coupling of the 20 AAs, which requires hundreds of experiments (**Figure 3**). While optimized for our process, the pipeline can quickly be adapted to any in situ synthesis approach, based on other printing technologies.

Initially, we needed a robust quantification procedure of the resulting AA spots (spot morphology and yield). A commonly used approach for the detection of AAs on functionalized surfaces is by fluorescence labeling and imaging. We investigated three different labeling procedures, such as direct dye labeling with or without side chain deprotection or indirect biotin-streptavidin labeling (Figure 3a; Figure S5, Supporting Information). We obtained reliable and comparable results by side chain deprotection of the AAs and direct DyLight 633 *N*-hydroxy-succinimide ester labeling. Furthermore, we assumed a positive correlation between fluorescence intensity and AA coupling efficiency: higher AA coupling results in higher fluorescence intensity (Figure S6, Supporting Information). This correlation was also previously observed by others.^[16] Moreover, to enable a fast analysis of thousands of fluorescent spots from various experiments (e.g., transfer parameters of 20 AAs), we developed an automated image detection software based on the open-source framework OpenCV.^[30]

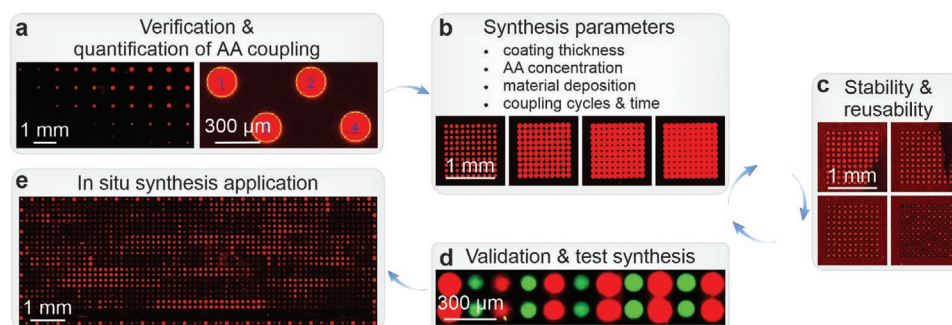


Figure 3. Optimization pipeline for the laser-based in situ peptide microarray synthesis. a) Verification and quantification of AA coupling is achieved by fluorescence labeling of amino groups and automated spot detection. b) To obtain an optimal spot size and synthesis yield, parameters such as styrene-acrylic copolymer coating thickness, AA concentration, and AA dependent material deposition, as well as AA coupling cycles and time are investigated. c) Afterward, the stability and reusability of all AAs is assessed and d) a validation synthesis is performed to determine the synthesis quality and yield of the found parameter sets. After several iterations, optimal parameters are obtained for all AAs, e) which can be used for various applications (e.g., combinatorial peptide synthesis).

Next, we needed to precisely control the deposited material of each transferred AA, which defines the final spot size and shape. Thus, we optimized the polymer coating thickness and AA concentration of an example AA donor slide (Figure 3b; Figures S7,S8, Supporting Information). Styrene-acrylic copolymer (SLEC; Figure S9, Supporting Information) was chosen, because in contrast to other polymers (Figure S10, Supporting Information), it offers the most robust spot sizes resulting in the highest synthesis resolution of 10000 spots cm^{-2} . Alanine was selected as the representative AA, because solubility issues should first arise for small and unpolar AAs. We varied the amount of SLEC and AA for the preparation of donor slides between 18–31.5 mg SLEC with 6.7–11.7% w/w AA. Even higher amounts of SLEC and AA resulted in highly variable spot sizes, while being less material saving. For 27 mg of SLEC and 3 mg of AA, we observed the most robust transfer (<100 μm width). However, since different AAs lead to different glass transition temperatures of the SLEC composite,^[10] the same laser parameters lead to different spot widths for each AA. Therefore, by varying lasing power and duration in a range (50–120 mW and 3–12 ms) for each AA, we extracted the optimal experimental parameters (Figures S11–S15, Supporting Information). Finally, as repeating coupling cycles of the same AA is typically performed in solid-phase peptide synthesis to increase the synthesis yield, we initially assumed three repeating coupling cycles per AA necessary, with a standard coupling time of 60 min each.

Employing these synthesis parameters, we investigated the potential to store the donor slides over a duration of seven days and reuse identical donor slide positions up to six times (Figure 3c; Figure S16, Supporting Information). This significantly reduces material consumption and preparation time. As we compared the fluorescence intensity and spot size to a fresh transfer (i.e., single transfer after one day of storage), we observed the trend of decreasing intensity and spot size over storage time and number of reuses. Particularly, the number of reuses strongly depends on the amount of previously transferred material and the deformation of the donor slide that is influenced by the lasing parameters (i.e., strong lasing parameters result in strong deformation) and is not a result of AA denaturation (Figure S17–S30, Supporting Information).

As a criterion before discarding a donor slide, we introduced empirical thresholds that took the use of multiple (repeated) coupling cycles into account: For spot densities of 1600 spots cm^{-2} and 10000 spots cm^{-2} , we required a minimum of 60% and 50% of the average fluorescence intensity and spot area. These values guaranteed saturated fluorescence intensity (and assumed coupling) over the entire spot.

To validate our first optimization iteration, we synthesized HA and Flag epitope variants (4444 spots cm^{-2}), containing one additional C-terminal AA (YPYDVPDYAX and DYKD-DDDKX, X = one of 20 AA; Figure 3d; Figure S31, Supporting Information), and measured specific antibody binding. For the Flag epitope, we observed a quantifiable trend, because the antibody binding appeared independent of the C-terminal AA, while the HA epitope binding was strongly influenced by the C-terminal AA. Yet, Flag peptides with a C-terminal histidine, proline, arginine, and tryptophan showed a (potentially) poor coupling efficiency. To overcome these assumed shortcomings, we performed an additional optimization iteration: For the poorly coupling AA, we increased the AA concentration to 20% w/w and repeated the analysis of optimal process parameters. Then, we investigated the optimal number of coupling cycles for each of the 20 AA (Figure S32, Supporting Information), where we defined the optimal number as maximum fluorescence intensity and non-overlapping spots. Interestingly, while the spot area increased over repeating coupling cycles, we observed a decrease in fluorescence intensity for some AAs after reaching maximum within the previous cycle. Hence, we used this observation as stop criterion. Consecutively, we investigated different coupling durations. A reduction from 60 min to 10 min is possible without a loss in coupling efficiency (Figure S33, Supporting Information). Finally, as we observed varying spot sizes for different AAs that will result in varying peptide spot widths, we introduced a pre-patterning of the acceptor slide with aspartic acid (Figure S34, Supporting Information). This restricted the growing peptide to the size of the initial aspartic acid spot pattern. We chose aspartic acid, because its negative charge at neutral pH is known to prevent unspecific interaction between most antibodies and the surface^[31] and the transfer resulted in small and stable spots after coupling.

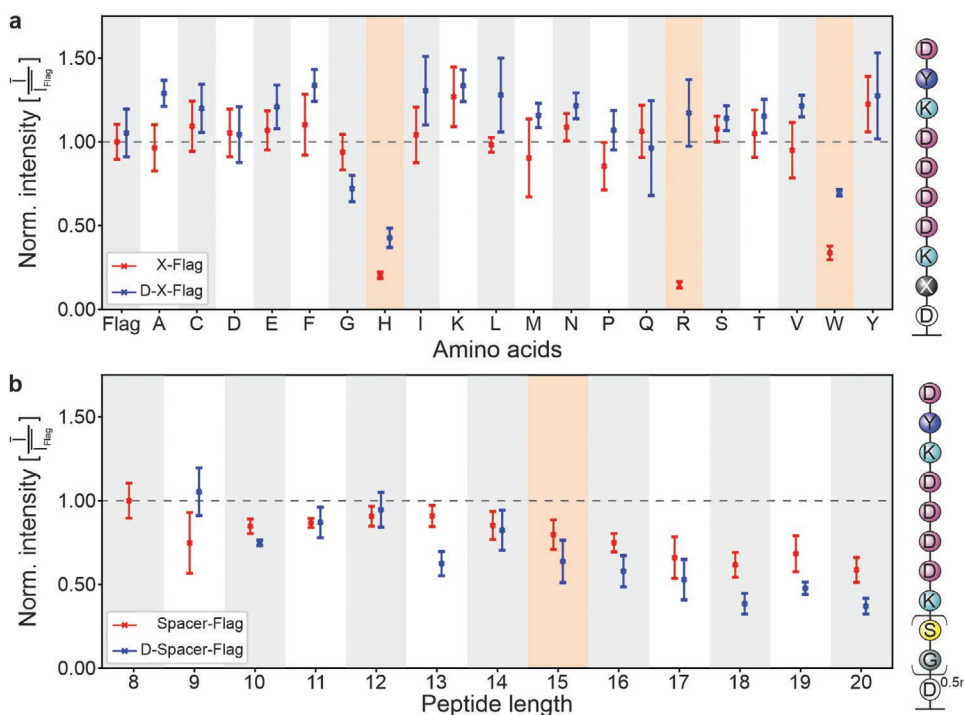


Figure 4. Validation of synthesis yield via antibody binding fluorescence analysis of a peptide microarray ($1600 \text{ spots cm}^{-2}$). Peptides were synthesized without and with aspartic acid pre-patterning. a) Intensities of the synthesized Flag peptides with an additional C-terminal AA of the 20 AAs. Histidine, arginine, and tryptophan show low binding, which is improved by aspartic acid pre-patterning. b) Flag peptides synthesized with a C-terminally growing glycine-serine spacer, resulting in up to 20-residue peptides. Fluorescence intensities are normalized against the wild-type Flag epitope (I_{Flag}) and presented as mean \pm SD, $n = 3$.

2.3. Validation of Optimized Parameters

Using the optimized parameters, we synthesized a microarray with $1600 \text{ spots cm}^{-2}$ containing Flag epitopes variants with an additional C-terminal AA, a 1–12 AA long glycine-serine spacer,^[32] and an aspartic acid pre-patterning. The variants with the 20 different AAs at the C-terminus still showed a decreased antibody binding for histidine, arginine, or tryptophan (Figure 4a). However, antibody binding increased after including the pre-patterning. This indicates that the coupling of these AAs can be strongly affected by the preceding AA, which has previously been reported.^[33] In comparison, variants with an increasing glycine-serine spacer without (Figure 4b) and with (Tables S1 and S2, Supporting Information) a C-terminal AA inclusion showed an expected behavior: The elongated Flag epitope (max. 20 residues) had an almost stable antibody binding up to a length of 15 residues. Then, a linear decrease to $\approx 59\%$ and $\approx 32\%$ without and with the pre-patterning was observed (compared to the reference peptide). This corresponds to an average yield of $\approx 95.7\%$ and $\approx 90.2\%$ respectively. Furthermore, we could verify that the minimal Flag epitope, which is responsible for the antibody recognition, is located at the N-terminus (Figure S35, Supporting Information). This is further supported by the performed Flag epitope substitution analysis (Figure S36, Supporting Information). Thus, due to this N-terminal epitope region, we could validate our 20-residue peptide microarray synthesis. In addition, we synthesized microarrays containing the same Flag variants with a spot density of $10000 \text{ spots cm}^{-2}$ and repeated our evaluation (Figure S37,

Tables S3 and S4, Supporting Information). A lower antibody binding was evident compared to the $1600 \text{ spots cm}^{-2}$ microarray synthesis. Nevertheless, sufficient antibody binding could be measured for most synthesized peptides. To support our assumption that the antibody binding correlates with the AA coupling efficiency, we analyzed the synthesis yield of representative AAs by measuring the N-(9H-Fluoren-9-ylmethyl)-piperidine absorbance after transferring one large AA spot pattern. While the measurement correlates with the antibody binding trend (e.g., low yield histidine, high yield glycine), it appeared less reliable (Figure S38, Supporting Information). Fluctuating synthesis yields between different acceptor slides were observed, which are strongly dependent on the coupled area (i.e., spot size upon labeling). Depending on this, the results varied up to $\approx 60\%$.

2.4. Validation and Application of the Laser-Assisted Peptide Synthesis

To validate our optimized parameter sets (Tables S5–S7, Supporting Information) for an application, we performed a fully combinatorial peptide microarray synthesis with 1600 , 4444 , and $10000 \text{ spots cm}^{-2}$. The Ebola virus surface glycoprotein was mapped as 662 individual 15-residue peptide spots with a lateral shift of one AA, which we used to screen the serum IgG antibody response of an Ebola virus disease survivor (Figure 5b and c). The IgG response of the three microarrays with different spot densities displayed a strong monotonic

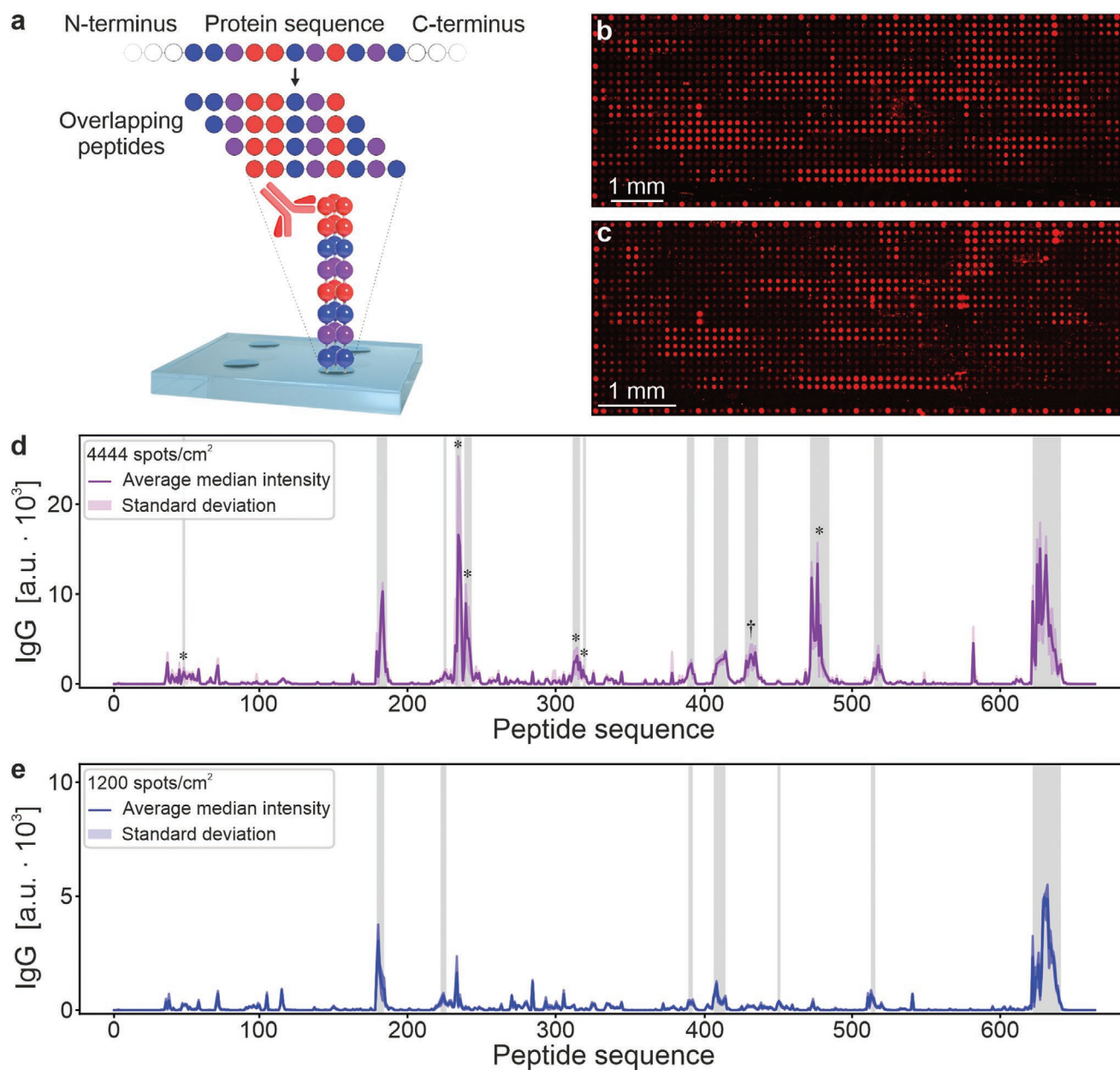


Figure 5. Synthesized Ebola virus surface glycoprotein peptide microarrays for IgG antibody screening of a disease survivor. a) The Ebola virus surface glycoprotein sequence was mapped as 662 overlapping 15-residue peptides with a lateral shift of one AA (as spot duplicates). After serum incubation, antibody binding to arrays with b) 4444 and c) 10000 spots cm⁻² was analyzed with fluorescence imaging and data presented as mean (of median IgG value) ± SD. d) The resulting signals of the 4444 spots cm⁻² ($n = 10$, background subtraction of 400 a.u.) and e) commercial reference microarrays ($n = 8$, background subtraction of 162 a.u.) are shown. Our synthesized microarray was able to detect more epitopes than the commercial array. Epitopes are highlighted in grey (*: known from literature; †: newly identified).

correlation (Figure S39, Supporting Information), which shows that our process is sufficiently robust to detect IgG epitopes independent of the spot density.

Next, to validate if we not only produced consistent microarrays but also detected significant epitopes, we screened the IgG response of an Ebola virus disease survivor on a commercial reference peptide microarray (produced with particle-based synthesis) containing the same peptides of the Ebola virus surface glycoprotein. This comparison showed that we could identify the same IgG epitopes as the commercial reference

(Table S8, Supporting Information), except for one minor signal (Figure 5d,e). Additionally, we found four previously reported epitopes,^[34,35] as well as one to our knowledge unreported epitope (AA 430–448), which highlights that we can produce fully combinatorial high quality peptide microarrays. Subsequently, we synthesized microarrays of the complete Ebola virus proteome in single AA resolution (4805 individual peptides) on separate 8.18 × 13.36 mm² and 4.54 × 10.70 mm² areas to perform a comprehensive epitope study of the Ebola virus disease survivor (Figures S40–S47 and Tables S8–S15, Supporting

Information). This was only possible with our increased microarray spot density, since a larger array surface area requires a higher than usually available amount of such a valuable serum sample. While the analysis of the complete Ebola proteome with peptide arrays has not been reported yet, our data coincide well with Becquart et al.,^[35] who have analyzed VP35, VP40, nucleoprotein, and glycoprotein with a peptide ELISA assay.

2.5. Laser-Based Synthesis of Fluorophore Microarrays

To show the chemical flexibility of our process and its capability to precisely tune the transferred material, we produced fluorophore microarrays (Figure 6). Besides the amide bond formation, we performed the Schiff base condensation reaction (imine formation) to synthesize a fluorophore array (Figure 6a). The Schiff base reaction can be used to synthesize various molecules^[36] or materials,^[37] such as fluorescent dyes for sensing applications.^[38,39] This makes them a highly attractive class of small molecules, which may be explored in microarray screenings. To synthesize the 2-((3-(carboxymethoxy)benzylidene)amino)benzoic acid on the microarray (Figure 6b), we carried out two steps: 1) Laser transfer and amide bond coupling of pentafluorophenyl activated 2-(3-formylphenoxy)acetic acid to the functionalized substrate 2) and consecutive laser transfer and Schiff base reaction of 2-aminobenzoic acid with 2-(3-formylphenoxy)acetic acid.

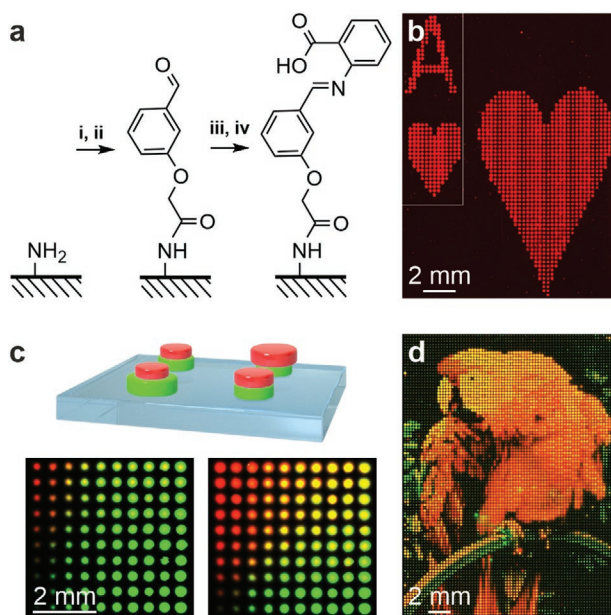


Figure 6. Laser-based synthesis of fluorophore microarrays. a-i,ii) Pentafluorophenyl activated 2-(3-formylphenoxy)acetic acid was transferred and coupled for 10 min at 95 °C to the surface via amide bond formation. iii,iv) 2-aminobenzoic acid was transferred and reacted for 90 min at 90 °C, forming the Schiff base 2-((3-(carboxymethoxy)benzylidene)amino)benzoic acid. b) Fluorescence image of the synthesized Schiff base microarray. c) Experimental screening of laser transfer parameters for two fluorescent dyes in SLEC (green: Rhodamine 6G, red: Nile blue A) to obtain a precise red-green color mixing (resulting in yellow). d) Optimal parameters enable the production of a 75 × 100 pixel (i.e., spot) image with thousands of different color ratios.

Moreover, we exploited the high precision of our system to precisely transfer defined amounts of SLEC containing red and green fluorophores onto a standard glass slide (Figure 6c,d). Recently, Whitesides et al. used inkjet printing to create fluorescent patterns for long-term data storage.^[40] While the authors required seven different dyes to store 8-bit information in one pixel, in our approach, we can create >256 distinguishable ratios in one spot by using only two fluorophores. To achieve this, we screened many nested laser parameter gradients (Figure S48, Supporting Information) to obtain optimum parameters for a precise red-green color mixing. Beyond data storage, this approach can enable the transfer of different chemicals in the microarray format for high-throughput reaction screening.

3. Conclusion

We developed a modular and robust automated high-throughput and high-precision laser-based microarray synthesizer that can generate up to 20-residue peptides with a spot density of 10 000 spots cm^{-2} in high yield. We established an analysis pipeline (material transfer, visualization, and quantification) to optimize our laser-based process in regards to transfer precision and reproducibility, as well as the resulting spot morphology and coupling efficiency. Through this optimization, we were able to advance our technology to synthesize thousands of different high quality peptides containing all 20 AAs and up to 20 residues. We synthesized 1600, 4444, and 10 000 spots cm^{-2} peptide microarrays containing the Ebola virus surface glycoprotein and analyzed the IgG response of an Ebola virus disease survivor. The results showed a high reproducibility with robust epitope detection, independent of the spot density. Compared to a commercial reference Ebola virus surface glycoprotein microarray, we not only identified the same epitopes with improved signal to noise ratio, but also detected additional epitopes that are known from literature using ELISA peptide screening platforms. These results imply that we achieve high quality syntheses. High-density peptide microarrays (4444 and 10 000 spots cm^{-2}) containing the complete Ebola virus proteome for the first time in single amino acid resolution (4805 individual peptides) provide an excellent tool to study the IgG response of an Ebola virus infection survivor. We illustrate the chemical flexibility of our process and its capability to precisely tune the amounts of transferred material by synthesizing a Schiff base fluorophore microarray. We refined the transfer for a highly precise mixing of two compounds, enabling high-throughput reaction screening in the microarray format. In the future, we will combine the automated system that drastically reduces manual labor,^[25,41] with our recently developed high-resolution donor slide,^[42] for automated microarray syntheses with densities of >100 000 spots cm^{-2} .

4. Experimental Section

Laser-Based Synthesizer. The lasing system consisted of a 405 nm wavelength diode laser with a Gaussian beam profile and a maximum of 300 mW power (iBeam smart 405-S, TOPTICA Photonics AG), which is lead through a laser scanning system (intelliSCAN III 10, SCANLAB),

linked to an f-theta-lens (JENar 170-355-140, JENOPTIK Optical Systems GmbH). The measured maximum power in the actual lasing area was 210 mW.

The transport of acceptor and donor slides was automated between the slide holder and the lasing area with a KUKA AGILUS six KR 3 R540 robot (KUKA AG), which has a precision of 20 μm and maximum axis velocities of A1:530, A2:529, A3:538, A4:600, A5:600, and A6:800 per s. To guarantee a stable process, each axis was reduced to 20% of its maximum possible velocity. As robot tool, a gripper (with four 2 mm diameter rubber suction cups) was used, which was connected to a pneumatics system that initiated and released vacuum for transportation.

Within the lasing area, a simple pressure based mechanical alignment, was introduced controlled by the pneumatics system, which ensured the same (<10 μm precision^[43]) acceptor slide position for every laser transfer. In specific, after the robot placed the acceptor slide into the lasing area, a soft vacuum suction (-30 kPa) was applied to keep the acceptor slide level. Then, pneumatic springs with curved bolts placed the acceptor slide into the desired location. A strong vacuum (-80 kPa) suction was applied to keep the acceptor slide in place during the process.

Finally, the entire setup (laser scanning system, transportation robot, pneumatics system, time management, etc.) was controlled through a self-designed control system.^[44] A python-based application that uses the RoboDK python API (version 3.4.7, RoboDK) was built to control the transportation robot and remote control laserDESK application (version 1.4.3.1, SCANLAB GmbH) to control the laser scanning system. The pneumatics systems and safety control was read out through a serial connection and in addition to the automation procedure, a graphical user interface was developed for non-expert use.

Evaluation of Amino Acid and Peptide Spots: The measured average fluorescence intensity of an AA spot was calculated through the averaged vertical and horizontal line intensity (obtained through ImageJ^[45]) and automatically evaluated threshold values that detect the spot edge. This approach guaranteed a measurement error below ± 2 pixel = ± 10 μm . Furthermore, the average AA spot area was approximated through the vertical and horizontal width to obtain the lowest spot area in case of deformation (i.e., worst-case approximation).

Automatically detected peptide spots of the produced microarrays were evaluated with a developed spot detection program,^[46] which resulted a maximum error of ± 4 pixel = ± 20 μm .

Measured peptide spots of the produced microarrays with a fixed spot size were evaluated with the GenePix Pro software (version 7 Analysis Only, Molecular Devices, LLC.). If not stated otherwise, a fixed feature (spot width) of 55, 90, and 110 μm was used for the evaluation of microarrays with a spot density of 1600, 4444, and 10000 spots cm^{-2} .

Commercial microarrays were evaluated with the PepSlide Analyzer software (version 1.5.8, SICASYS Software GmbH) using the fixed-spot detection method with a spot width of 250 μm and spot height of 400 μm . The printed region was 190 μm \times 338 μm .

Donor Slide Preparation: For the preparation of a blank donor slide, a microscope glass slide was covered with self-adhesive polyimide foil (Kapton HN, DuPont, 25 μm polyimide layer with a 45 μm siloxane-based adhesive layer; CMC Klebtechnik), which acted as a support. Then, different mixtures of styrene acrylic copolymer (SLEC; SLEC LT 7552, Sekisui Chemical CO., LTD), pre-dissolved in 450 μL dichloromethane (DCM), and a chemical compound, pre-dissolved in 50 μL *N,N*-dimethylformamide (DMF), which resulted in 500 μL of spin coating solution, were prepared. These solutions were spin-coated (80 rps) on top of a blank donor slide resulting in a variety of donor slide compositions (Table S16, Supporting Information). Materials, spin coating parameters, and resulting theoretical coating thicknesses (Tables S17 and S18, Supporting Information) were derived from Danglad-Flores et al.^[47,48]

Acceptor Slide Preparation and Amino Acid Coupling: For the peptide microarray synthesis, PEGMA-co-MMA (PEPperPRINT GmbH) slides with a terminal *N*-[(9*H*-Fluoren-9-ylmethoxy)carbonyl]-protected (Fmoc-protected) β -alanine were used as solid support (acceptor slides). All

solvent incubation steps were carried out at room temperature (rt). Furthermore, for every solvent incubation step, the acceptor slide was placed in a petri dish, fully covered with solvent, and vibrated on an orbital shaker.

Pre-swelling of the PEGMA-co-MMA coating was achieved by immersing the acceptor slide in DMF for 20 min. For Fmoc-deprotection the acceptor slide was immersed in 20% v/v piperidine in DMF for 20 min. After washing the acceptor slide 3 \times for 3 min in DMF, 1 \times for 2 min in methanol (MeOH), and 1 \times for 1 min in DCM (in the following called wash), it was dried in a jet of air.

Following laser-assisted material transfer, the coupling reaction was performed: By heating the acceptor slide to 95 $^{\circ}\text{C}$ for 60 min under inert gas atmosphere, the pentafluorophenyl ester-activated (OPfp-activated) AA reacted with the functional groups of the acceptor slide. If not stated otherwise, AAs were Fmoc-protected and OPfp-activated (Novabiochem, Merck KGaA). Due to the OPfp activation of the AAs, a low rate of racemization was expected,^[49] which have been shown for cysteine (Figures S48 and S49, Supporting Information) and tyrosine (Figures S50 and S51, Supporting Information).

Direct Labeling of Amino Groups with a Fluorescent Dye: The acceptor slide preparation protocol, as described in *acceptor slide preparation and amino acid coupling*, was followed. After the AA was transferred and coupled, the remaining amino groups of the acceptor slide were capped twice by immersing the slide in a solution of 10% acetic anhydride, 20% *N,N*-diisopropylethylamine (DIPEA), and 70% DMF v/v/v. The first capping cycle included 2 min in an ultrasonic bath, followed by 30 min on a shaker. The second cycle was carried out with a fresh capping solution for 30 min. Then, the slide was washed and dried. Afterwards, the Fmoc-protected amino groups of the AAs were deprotected (*acceptor slide preparation and amino acid coupling*) and the slides were washed and dried. For AAs with protected side chains, the acid labile protecting groups were deprotected by immersing the acceptor slide 3 \times for 30 min in a solution of 51% trifluoroacetic acid (TFA), 44% DCM, 3% triisobutylsilane, and 2% water v/v/v/v. Next, the acceptor slide was washed for 5 min in DCM and then, immersed in 5% v/v DIPEA in DMF for 20 min. Following side chain deprotection and neutralization, the acceptor slide was washed and dried. Next, to visualize the resulting AA spots, the amino groups were stained with DyLight 633 *N*-hydroxysuccinimide ester (NHS; Thermo Fisher Scientific Inc.). The acceptor slide was immersed in 0.05% v/v Tween 20 (Sigma-Aldrich) in phosphate-buffered saline (PBST) containing 0.1 $\mu\text{g mL}^{-1}$ DyLight 633 NHS ester for 60 min. Finally, the slide was rinsed with water, washed 2 \times for 10 min in PBST, rinsed multiple times with water, washed 2 \times for 10 min in DMF, washed 1 \times for 1 min with DCM, and dried.

Indirect labeling of amino groups with biotin and streptavidin: The acceptor slide preparation protocol and AA coupling (*acceptor slide preparation and amino acid coupling*), capping, and deprotection were carried out (direct labeling of amino groups with a fluorescent dye). Subsequently, 250 μL of a solution containing 20 $\mu\text{mol mL}^{-1}$ biotin (Fluka BioChemika), 60 $\mu\text{mol mL}^{-1}$ *N,N'*-diisopropylcarbodiimide (DIC; Acros Organics B.V.B.A), and 20 $\mu\text{mol mL}^{-1}$ pentafluorophenol (PfpOH; Acros Organics B.V.B.A) in DMF were carefully spread on one acceptor slide. A second acceptor slide was placed on top of the first to functionalize both simultaneously overnight. Afterward the slides were washed and dried. To avoid unspecific binding, the acceptor slide was blocked with blocking buffer (MB-070, Rockland Immunochemicals Inc.) for 30 min on a shaker. Next, the slide was incubated with 0.4 $\mu\text{g mL}^{-1}$ CF633 streptavidin (29037, Biotium, Inc.) in staining buffer (10% v/v blocking buffer in PBST) for 60 min on a shaker. Finally, the acceptor slide was shortly washed 3 \times with PBST, dipped in 1 mmol L^{-1} tris(hydroxymethyl) aminomethane (Tris) buffer (Carl Roth GmbH + Co. KG) with pH 7.4, and dried in a jet of air.

Reversed-Phase High Performance Liquid Chromatography Coupled to Mass Spectrometry of Single AA: To analyze the potential of AA denaturation during laser-assisted transfer, reversed-phase high performance liquid chromatography (RP-HPLC) coupled to mass spectrometry (MS) measurements of valine, phenylalanine, and tyrosine (reuse values of 2, 4, and 6 respectively) were performed. The

AA were transferred over an area of $20 \times 60 \text{ mm}^2$ onto microscope glass slides and then, heated for 10 min. New and reused donor slides were used separately for the transfer onto the microscope glass slides. Following laser-assisted transfer and heating, the material was washed from the glass slides with acetone and dried in a Buchi Rotavapor R-210. Additionally, measurements of phenylalanine after five cycles of transferring and heating were performed to investigate the influence of above optimal coupling cycles. References of each AA were also analyzed, as well as transferred SLEC, which is present in all transferred samples. Following laser-assisted transfer and heating, the material was washed from the glass slides with acetone and dried in a Buchi Rotavapor R-210. Samples containing AA and SLEC were dissolved in $100 \mu\text{L}$ of dioxane. AA references were diluted to 0.5 mg mL^{-1} in dioxane. RP-HPLC-MS was performed with an Agilent Technologies 1260 Infinity II coupled to InfinityLab LC/MSD single quadrupole mass spectrometer. For separation of the AA SLEC mixture, the following methods were used—method A: Agilent InfinityLab Proshell 120 EC-C18, $3.0 \times 150 \text{ mm}$, $2.7 \mu\text{m}$, flow rate 0.7 mL min^{-1} with 5 min 50% B in A, 50% to 100% B in A in 35 min, 5 min 100% B, (A = 0.1% formic acid in water, B = acetonitrile).

Peptide Array Synthesis—Acceptor Slide Modification: First, a PEGMA-co-MMA Fmoc- β -alanine acceptor slide was pre-swollen, deprotected, washed, and dried (*acceptor slide preparation and amino acid coupling*). For the Ha and Flag epitope syntheses, $250 \mu\text{L}$ of a solution containing $20 \mu\text{mol mL}^{-1}$ OPfp-activated Fmoc-protected aspartic acid in DMF were carefully spread on top of one acceptor slide and a second acceptor slide was placed on top to functionalize both slides simultaneously overnight. In contrast, for the produced Ebola virus surface glycoprotein/proteome peptide microarrays, the aforementioned step was replaced by laser-assisted material transfer and coupling of the OPfp-activated Fmoc-protected aspartic acid (i.e., pre-patterning). Subsequently, the slides were washed, dried, capped twice (*direct labeling of amino groups with a fluorescent dye*), washed, dried, Fmoc-deprotected (*acceptor slide preparation and amino acid coupling*). Then, washed and dried again. Likewise, a second functionalization step with a solution containing $20 \mu\text{mol mL}^{-1}$ Fmoc-protected β -alanine, $60 \mu\text{mol mL}^{-1}$ DIC, and $20 \mu\text{mol mL}^{-1}$ hydroxybenzotriazole (HOBt; Sigma-Aldrich) was performed and again, the slides were washed, dried, capped twice, washed, and dried.

Peptide Array Synthesis—Coupling Reaction: A PEGMA-co-MMA β -alanine aspartic acid Fmoc- β -alanine functionalized slide was used (*peptide array synthesis—acceptor slide modification*). The slide was pre-swollen, Fmoc-deprotected, washed, dried, and the AAs transferred and coupled (*acceptor slide preparation and amino acid coupling*). The laser-assisted transfer of AA patterns from different donor slides to the acceptor was performed, followed by coupling at $95 \text{ }^\circ\text{C}$ for 60 min (or 10 min for the Ebola virus surface glycoprotein/proteome microarrays) under inert gas atmosphere. Before the laser-assisted transfer of all AAs was repeated with identical patterns, the acceptor slide was washed 2 \times in acetone for 2 min and dried. After completion of all coupling cycles (coupling of one AA layer), two capping cycles (for the first AA layer three times) were carried out (*direct labeling of amino groups with a fluorescent dye*). From the third AA layer on, the capping duration was reduced to 15 min per capping cycle. Next, the acceptor slide was Fmoc-deprotected (*acceptor slide preparation and amino acid coupling*), washed, and dried. The aforementioned steps (laser-assisted transfer, coupling, capping, and Fmoc-deprotection) were repeated to synthesize the desired peptides in the array format. Then, the N-terminus of the peptide was acetylated (*direct labeling of amino groups with a fluorescent dye*) and the slides were washed and dried. Concluding the peptide synthesis, the side chains of the AAs were deprotected (*direct labeling of amino groups with a fluorescent dye*), neutralized, washed, and dried.

HA and Flag Epitope Array Staining: The synthesized HA and Flag epitope arrays were detected with ReadyTag anti-HA (RT028, Bio X Cell, Inc.; 1.0 mg mL^{-1}) labeled with Lightning-Link Rapid Cy5 Labeling Kit (342-0005, Expedeon Ltd.) and Anti-Flag M2-Cy3 (A9594, Sigma-Aldrich; 1.0 mg mL^{-1}). To avoid unspecific binding of the serum antibodies, the arrays were blocked with blocking buffer for 30 min with orbital shaking.

Subsequently, the arrays were incubated with 1:1000 diluted anti-HA and/or anti-Flag antibodies in staining buffer for 30 min on a shaker. To remove unbound antibodies, the arrays were shortly washed 3 \times with PBST. Finally, the arrays were dipped in 1 mmol L^{-1} Tris HCl buffer pH 7.4 and dried in a jet of air.

For the validation of synthesis yield via antibody binding fluorescence analysis by peptide microarray (Figure 4), the negative controls (i.e., copies of all synthesized peptides with an additional C-terminal SLEC spot without any AA) were $\approx 10\%$ of the wild type Flag epitope.

Coupling Analysis of Amino Acids via N-(9H-Fluoren-9-ylmethyl)-piperidine Absorbance: The following procedure was adapted from Loeffler et al.^[14] For pre-swelling, 1 mL of DMF was pipetted onto an acceptor slide and incubated for 20 min. To avoid evaporation, a tissue, moisturized with DMF, was placed inside the petri dish. Then, Fmoc-deprotection was performed by replacing the DMF with 1 mL of 20% v/v piperidine in DMF and incubation for 20 min. The deprotection solution was collected and the acceptor slide rinsed with additional $200 \mu\text{L}$ 20% v/v piperidine in DMF, which were collected as well. The absorbance of N-(9H-Fluoren-9-ylmethyl)-piperidine at 301 nm within the deprotection solution was measured to determine the loading of the acceptor slide with β -alanine. After the acceptor slide was washed and dried in a jet of air, a large AA pattern was transferred onto this acceptor slide and coupled for 10 min at $95 \text{ }^\circ\text{C}$ under inert gas atmosphere. The slide was capped 2 \times for 20 min and 1 \times for 30 min with a fresh solution of 10% acetic anhydride, 20% DIPEA, and 70% DMF v/v/v, as well as washed and dried in a jet of air. Consecutively, the Fmoc-deprotection and absorbance measurement (at 301 nm) were repeated. Finally, to calculate the loading after AA transfer, the coupled area was detected by labeling with DyLight 633 NHS ester (*direct labeling of amino groups with a fluorescent dye*). Loading formula: $\text{loading} \left[\frac{\text{nmol}}{\text{cm}^2} \right] = \frac{E V 10^6}{d \epsilon A}$

(E: measured extinction; V: volume [mL], 1.2 mL ; d: distance [cm], 1 cm ; ϵ : molar absorption coefficient [$\text{L mol}^{-1} \text{ cm}^{-1}$], $5129 \text{ L mol}^{-1} \text{ cm}^{-1}$; A = area [cm^2], 19.76 cm^2 or measured).

Ebola Virus Proteome Array Generation and Patient Sample Analysis: For the generation of the Ebola virus proteome arrays, the NCBI reference sequence NC_002549.1 was used and cut into overlapping 15-residue peptides, which were synthesized on the arrays. Prior to the incubation with serum (Ebola virus disease survivor, voluntary donor with informed consent,^[50] as agreed with the ethics committee of the Goethe University Hospital, Frankfurt), the arrays were incubated with the subsequently explained steps, including the secondary antibodies without the use of a serum sample. This was carried out to monitor unspecific binding of the secondary antibodies to the peptide arrays (false positive signals).

Before incubation, the arrays were pre-swollen for 15 min with PBST at rt and orbital shaking. To avoid unspecific binding of the serum antibodies, the arrays were blocked with blocking buffer for 30 min with orbital shaking. Following a short washing step with PBST, 1:200 diluted serum in staining buffer was incubated overnight with shaking at $4 \text{ }^\circ\text{C}$. To remove unbound serum components, the arrays were shortly washed 3 \times with PBST. Next, the human serum antibodies were detected with 1:1000 diluted Anti-Human IgG Fc cross-adsorbed DyLight 650 (A80-304D5, Bethyl Laboratories, Inc., USA; 0.5 mg mL^{-1}), 1:2000 diluted Anti-Human IgM ($m\mu$ chain) DyLight 549 (609-142-007, Rockland Immunochemicals, Inc.; 1.0 mg mL^{-1}) in staining buffer. In parallel, control peptides were detected with 1:2000 diluted anti-HA and anti-Flag in staining buffer. Thus, the diluted secondary antibodies were applied simultaneously to the microarrays for 30 min at rt and orbital shaking. Finally, to remove unbound secondary antibodies, the arrays were shortly washed 3 \times with PBST, dipped in 1 mmol L^{-1} Tris HCl buffer pH 7.4, and dried in a jet of air.

Vertical Scanning Interferometry: Vertical scanning interferometry was performed with a smartWLI compact (Gesellschaft für Bild- und Signalverarbeitung (GBS) GmbH, Ilmenau, Germany) attached to a 5 \times magnification lens. Resulting measurements were evaluated with the developed spot software.^[46]

Size Exclusion Chromatography: Size exclusion chromatography was conducted in tetrahydrofuran (VWR, ACS grade, predistilled) with

toluene as internal standard at 25 °C using a column system by PSS SDV 100/1000/100000 column (8 × 300 mm, 5 μm particle size) with a PSS SDV precolumn (8 × 50 mm), a SECcurity RI detector, SECcurity UV/VIS detector, and a calibration with PS standards or PEO standards from PSS.

Reversed-Phase High Performance Liquid Chromatography Coupled to Mass Spectrometry of Peptide Epimers: To analyze potential racemization of AAs during peptide synthesis, RP-HPLC-MS measurements of short 4-residue peptides (CFDD and YFDD) were performed. Either Fmoc-Cys(Trt)-OPfp or Fmoc-Tyr(tBu)-OPfp in DMF (0.1 mmol/mL) were coupled at 95 °C for 15 min (ensuring at least 10 min at 95 °C) to Rink amide resin (855001, Novabiochem Merck), carrying 3-residue peptide (FDD), in a 1.5 mL reaction tube using an Eppendorf ThermoMixer C. The prepared peptides were Fmoc-deprotected and cleaved from the solid support with simultaneous deprotection of side chain groups by using 90% TFA, 5% triisopropylsilane, 5% water v/v/v for 2 h. Cold diethyl ether was added to the crude peptide containing solution and cleaved product solution and after 30 min on ice, the supernatant was decanted after centrifugation. This process was repeated and the crystallized product was dried. Finally, the product was dissolved in water and lyophilized with Christ Alpha 2-4 LD plus freeze dryer.

For the analysis, the peptides were dissolved in water. The references containing a 1:1 mixture of L-CFDD and D-CFDD or L-YFDD and D-YFDD were diluted to 0.5 mg mL⁻¹ in water. RP-HPLC-MS was performed with an Agilent Technologies 1260 Infinity II coupled to InfinityLab LC/MSD single quadrupole mass spectrometer. For separation of the L/D-peptide epimers, method B: Agilent InfinityLab Proshell 120 EC C18, 3.0 × 150 mm, 2.7 μm, flow rate 0.7 mL min⁻¹ with 5 min 100% A, 0% to 60% B in A in 35 min, 5 min 60% B (A = 0.1% formic acid in water, B = acetonitrile), was used.

NMR Spectroscopy: The NMR spectra were measured at rt and recorded on a Varian 400-MR (400 MHz; Varian Medical Systems) or Bruker Ascend 400 (400 MHz; Bruker Corporation) spectrometer. Chemical shifts δ were reported in ppm and adjusted to internal standards of the residual proton signal of the deuterated solvent (CDCl₃: 7.26 ppm for ¹H and 77.0 ppm for ¹³C; D₂O: 4.80 ppm for ¹H; DMSO-d₆: 2.50 ppm for ¹H and 39.52 ppm for ¹³C). The center of the signal was given for symmetrical signals and the area for multiplets. Thereby, the following common abbreviations were used for multiplicities: s = singlet, d = doublet, t = triplet, q = quartet, m = multiplet, or for combinations dd = doublet of doublet, dt = doublet of triplet, etc. Coupling constants (J) were given in Hz.

Mass Spectrometry: High-resolution mass spectrometry (HRMS) was performed on a 6210 ESI-TOF mass spectrometer (Agilent Technologies). The abbreviation [M+Na]⁺ referred to the product–sodium adduct. The abbreviation [M-H]⁻ refers to the product without a proton adduct.

Synthesis of Fluorophore 2-((3-(Carboxymethoxy)benzylidene)amino)benzoic Acid 3: 2-aminobenzoic acid 1 (137 mg, 1.00 mmol, 1.00 equiv.) and 2-(3-formylphenoxy)acetic acid 2 (216 mg, 1.20 mmol, 1.20 equiv.) were respectively dissolved in ethanol (5 mL) at rt. Afterward, the two prepared solutions were mixed under vigorous stirring (800 rpm). The mixture was heated to 60 °C for 180 min and then, cooled down to room temperature. Subsequently, the precipitations were respectively filtered and washed three times with ethanol and diethyl ether. The crude product was purified by flash chromatography using pure methanol as eluent. Finally, the product was obtained as a yellowish solid in 79% yield (237 mg, 790 μmol). For details, also see Figures S52 and S53 in the Supporting Information.

¹H-NMR (400 MHz, DMSO-d₆): δ = 4.89 (s, 2H, -CH₂COO), 7.06–7.21 (m, 3H, Ar), 7.41–7.60 (m, 3H, Ar), 7.72 (s, 1H, H-1), 7.84 (d, J = 7.6 Hz, 1H, Ha-2), 8.06 (d, J = 7.6 Hz, 1H, Hb-2), 8.96 (s, 1H, -CH=N-) ppm.

¹³C-NMR (101 MHz, DMSO-d₆): δ = 65.19, 113.36, 121.10, 124.09, 125.63, 126.68, 127.10, 129.68, 131.95, 133.37, 136.25, 152.25, 156.85, 158.11, 167.08, 170.04 ppm.

HRMS (ESI, m/z): calcd. for C₁₆H₁₄NO₅ [M-H]⁻: 300.0794; found: 300.0853.

Fluorescence Analysis of 2-((3-(Carboxymethoxy)benzylidene)amino)benzoic Acid: The 2D fluorescence spectrum of 2-((3-(carboxymethoxy)benzylidene)amino)benzoic acid (Figure S54, Supporting Information) was measured through the spectrofluorometer FP-8300 (JASCO Deutschland GmbH). The testing solution was prepared by dissolving 2-((3-(carboxymethoxy)benzylidene)amino)benzoic acid in methanol (analytical grade) with a final concentration of 75 μg mL⁻¹. The normal fluorescence spectra of 2-(3-formylphenoxy)acetic acid and 2-aminobenzoic acid were tested with the same procedure at a fixed excitation wavelength of 532 nm (Figure S55, Supporting Information).

Computational Simulation of 2-((3-(Carboxymethoxy)benzylidene)amino)benzoic Acid: The simulation was performed with GaussView 5.0 and Gaussian 09. Molecular orbital amplitude plots of 2-((3-(carboxymethoxy)benzylidene)amino)benzoic acid for the highest occupied (HOMO) and lowest unoccupied molecular orbital (LUMO) were calculated through density functional theory with the B3LYP hybrid functional and a basis set level of 6-31G* (Figure S56, Supporting Information).

Fluorophore Microarray Synthesis Using the Schiff Base Reaction: Blank donor slides and spin-coating parameters were used as described in donor slide preparation. For the 2-(3-formylphenoxy)acetic acid donor slide, 27 mg SLEC was pre-dissolved in 450 μL DCM and then, mixed with 50 μL DMF containing DIC (2.78 mg, 22.0 μmol, 1.00 equiv.), PfpOH (7.00 mg, 38.0 μmol, 1.73 equiv.), and 2-(3-formylphenoxy)acetic acid 2 (4.00 mg, 22.0 μmol, 1.00 equiv.; 152153, Sigma-Aldrich). The 2-aminobenzoic acid donor slide was prepared by simultaneously dissolving 27 mg SLEC and 10 mg 2-aminobenzoic acid 1 (A89855, Sigma-Aldrich) in 500 μL acetone.

Next, the acceptor slide preparation protocol, as described in acceptor slide preparation and amino acid coupling, was followed. Consecutively, laser-assisted material (Table S19) transfer and the coupling reaction was performed: By heating the acceptor slide to 95 °C for 10 min under inert gas atmosphere, the OPfp-activated 2-(3-formylphenoxy)acetic acid 2 reacted with the functional groups of the acceptor slide. The material transfer and coupling procedure was performed three times. After each coupling, the acceptor slide was washed 3× for 5 min in MeOH and then dried in a jet of air. For 2-aminobenzoic acid 1, the material transfer was performed once and a coupling duration of 90 min was used. Finally, before fluorescence imaging (Figure 6b), the acceptor slide was washed 3× for 5 min in MeOH, 1× for 1 min in DCM, and dried in a jet of air.

Fluorescence Imaging: Fluorescence image acquisition for all experiments was performed with the fluorescence scanner Genepix 4000B (Molecular Devices) with a resolution of 5 μm and a laser power of 33%. The different parameters for the wavelength detection and photo multiplier gain (PMT) are listed in Table S20, Supporting Information.

Statistical Analysis: Data was acquired from unprocessed fluorescence image data. If applicable, applied transformations (e.g., normalization and background subtraction) are stated within the caption of each figure/table. Except for data points that were strongly affected by process irregularities (e.g., dirt), outliers were considered. Quantitative data was presented as measurement value ± measurement error, mean ± standard deviation (SD), or mean with min/max value boundaries. For all single AA experiments, the sample size was increased until a trend was observable. At least three data points per experiment were acquired, except for the evaluation of the proteome data that contained two data points. Statistical significance of the spearman rank correlation was assessed using python scipy.stats.spearmanr; a p-value of at least p < 10⁻¹⁰ was measured for all experiments. All statistical analyses were carried out with python and the developed analysis tools (Evaluation of amino acid and peptide spots). IgG epitopes within the Ebola virus proteome were detected by surpassing a threshold value that is based on the limit of blank, which were acquired from the fluorescence intensity of secondary antibodies. For the synthesized microarrays, the threshold value was at least ten times above the limit of blank.

Supporting Information

Supporting Information is available from the Wiley Online Library or from the author.

Acknowledgements

The authors thank E. Settels and O. Niemeyer for their technical assistance, K. Bienert, A. Kretzschmar, T. Schmidt, J. Petersen, and M. Bott for the construction of the automated synthesizer, A. Jacob (Peps4LS GmbH) for consulting and synthesis of peptides, and Manuel Garcia Ricardo for the discussions on peptide racemization. Funding was provided by the German Federal Ministry of Education and Research (13XP5050A), the MPG-FhG cooperation grant Glyco3Display, and the Max Planck Society.

Open access funding enabled and organized by Projekt DEAL.

Conflict of Interest

F.B. and F.F.L. are named on a patent application related to laser-based microarray synthesis. All other authors declare that they have no competing interests.

Author Contributions

G.P. and J.H. contributed equally to this work. Conceptualization: G.P., J.H., F.F.L.; Data curation: G.P., J.H.; Formal analysis: G.P., J.H.; Funding acquisition: F.F.L.; Investigation: G.P., J.H., A.T., Y.L., D.M., C.L., F.R.B.; Methodology: G.P., J.H., S.P.M., M.M.; Project administration: G.P., J.H.; Resources: R.W., C.R., P.H.S., F.B., T.W., F.F.L.; Software: G.P.; Supervision: F.B., F.F.L.; Validation: G.P., J.H., A.T., Y.L., D.M., S.P.M., P.D., M.M., F.F.L.; Visualization: G.P., J.H., A.T., Y.L.; Writing—original draft: G.P., J.H., F.F.L.; Writing—review and editing: G.P., J.H., D.M., M.M., C.R., P.H.S., F.F.L.

Data Availability Statement

The data that support the findings of this study are available in the supplementary material of this article.

Keywords

high-throughput, laser-induced forward transfer, peptides, Schiff base fluorophores, solid phase synthesis

Received: January 12, 2022

Revised: March 23, 2022

Published online: April 28, 2022

- [1] R. B. Merrifield, *Science* **1965**, 150, 178.
- [2] M. H. Caruthers, *Science* **1985**, 230, 281.
- [3] O. J. Plante, E. R. Palmacci, P. H. Seeberger, *Science* **2001**, 291, 1523.
- [4] J. Li, S. G. Ballmer, E. P. Gillis, S. Fujii, M. J. Schmidt, A. M. E. Pallazzolo, J. W. Lehmann, G. F. Morehouse, M. D. Burke, *Science* **2015**, 347, 1221.
- [5] H. M. Geysen, R. H. Meloen, S. J. Barteling, *Proc. Natl. Acad. Sci. U. S. A.* **1984**, 81, 3998.
- [6] R. Frank, *Tetrahedron* **1992**, 48, 9217.
- [7] S. P. Fodor, J. L. Read, M. C. Pirrung, L. Stryer, A. T. Lu, D. Solas, *Science* **1991**, 251, 767.
- [8] J. P. Pellois, X. Zhou, O. Srivannavit, T. Zhou, E. Gulari, X. Gao, *Nat. Biotechnol.* **2002**, 20, 922.
- [9] M. Beyer, A. Nesterov, I. Block, K. König, T. Felgenhauer, S. Fernandez, K. Leibe, G. Torralba, M. Hausmann, U. Trunk, F. R. Bischoff, V. Stadler, F. Breitling, *Science* **2007**, 318, 1888.
- [10] V. Stadler, T. Felgenhauer, M. Beyer, S. Fernandez, K. Leibe, S. Güttler, M. Gröning, K. König, G. Torralba, M. Hausmann, V. Lindenstruth, A. Nesterov, I. Block, R. Pipkorn, A. Poustka, F. R. Bischoff, F. Breitling, *Angew. Chem., Int. Ed.* **2008**, 47, 7132.
- [11] J. V. Price, S. Tangsombatvisit, G. Xu, J. Yu, D. Levy, E. C. Baechler, O. Gozani, M. Varma, P. J. Utz, C. Liu, *Nat. Med.* **2012**, 18, 1434.
- [12] S. Buus, J. Rockberg, B. Forsström, P. Nilsson, M. Uhlen, C. Schafer-Nielsen, *Mol. Cell. Proteomics* **2012**, 11, 1790.
- [13] J. B. Legutki, Z. Zhao, G. Greving, N. Woodbury, S. A. Johnston, P. Stafford, *Nat. Commun.* **2014**, 5, 4785.
- [14] F. F. Loeffler, T. C. Foertsch, R. Popov, D. S. Mattes, M. Schlageter, M. Sedlmayr, B. Ridder, F. X. Dang, C. v. Bojničić-Kninski, L. K. Weber, A. Fischer, J. Greifenstein, V. Bykovskaya, I. Buliev, F. R. Bischoff, L. Hahn, M. A. R. Meier, S. Bräse, A. K. Powell, T. S. Balaban, F. Breitling, A. Nesterov-Mueller, *Nat. Commun.* **2016**, 7, 11844.
- [15] C. Moreno-Yruela, M. Bæk, A. Vrsanova, C. Schulte, H. M. Maric, C. A. Olsen, *Nat. Commun.* **2021**, 12, 62.
- [16] W. Lin, S. Gandhi, A. R. Oviedo Lara, A. K. Thomas, R. Helbig, Y. Zhang, *Adv. Mater.* **2021**, 33, 2102349.
- [17] D. Shin, K. Lee, B. Yoo, J. Kim, M. Kim, Y. Kim, Y. Lee, *J. Comb. Chem.* **2010**, 12, 463.
- [18] JPT Peptide Technology GmbH, <https://www.jpt.com> (accessed: August 2021).
- [19] LC Sciences, <https://www.lcsciences.com> (accessed: August 2021).
- [20] PEPPERPRINT GmbH, <https://www.pepperprint.com> (accessed: August 2021).
- [21] A. Chandra, N. Latov, G. P. Wormser, A. R. Marques, A. Alaadini, *Clin. Immunol.* **2011**, 141, 103.
- [22] B. A. R. Williams, C. W. Diehnelt, P. Belcher, M. Greving, N. W. Woodbury, S. A. Johnston, J. C. Chaput, *J. Am. Chem. Soc.* **2009**, 131, 17233.
- [23] J. Tan, B. K. Sack, D. Oyen, I. Zenklusen, L. Piccoli, S. Barbieri, M. Foglierini, C. Silacci-Fregni, J. Marcandalli, S. Jongo, S. Abdulla, L. Perez, G. Corradin, L. Varani, F. Sallusto, B. K. L. Sim, S. L. Hoffman, C. Daubenberger, I. A. Wilson, A. Lanzavecchia, *Nat. Med.* **2018**, 24, 401.
- [24] M. Benz, A. Asperger, M. Hamester, A. Welle, S. Heissler, P. A. Levkin, *Nat. Commun.* **2020**, 11, 5391.
- [25] K. Heiss, J. Heidepriem, N. Fischer, L. K. Weber, C. Dahlke, T. Jaenisch, F. F. Loeffler, *J. Proteome Res.* **2020**, 19, 4339.
- [26] M. Koenig, C. Bentow, M. Satoh, M. J. Fritzer, J. Senécal, M. Mahler, *Rheumatology* **2019**, 58, 1784.
- [27] S. Eickelmann, A. Tsouka, J. Heidepriem, G. Paris, J. Zhang, V. Molinari, M. Mende, F. F. Loeffler, *Adv. Mater. Technol.* **2019**, 4, 1900503.
- [28] G. Paris, A. Klinkusch, J. Heidepriem, A. Tsouka, J. Zhang, M. Mende, D. S. Mattes, D. Mager, H. Riegler, S. Eickelmann, F. F. Loeffler, *Appl. Surf. Sci.* **2020**, 508, 144973.
- [29] S. Eickelmann, S. Ronneberger, J. Zhang, G. Paris, F. F. Loeffler, *Adv. Mater. Interfaces* **2021**, 8, 2001626.
- [30] OpenCV, Open Source Computer Vision Library **2015**, <https://opencv.org/> (accessed: April 2022).
- [31] A. Fukunaga, S. Maeta, B. Reema, M. Nakakido, K. Tsumoto, *Biochem. Biophys. Rep.* **2018**, 15, 81.
- [32] M. v. Rosmalen, M. Krom, M. Merx, *Biochemistry* **2017**, 56, 6565.
- [33] N. Hartrampf, A. Saebi, M. Poskus, Z. P. Gates, A. J. Callahan, A. E. Cowfer, S. Hanna, S. Antilla, C. K. Schissel, A. J. Quartararo, X. Ye, A. J. Mijalis, M. D. Simon, A. Loas, S. Liu, C. Jessen, T. E. Nielsen, B. L. Pentelute, *Science* **2020**, 368, 980.
- [34] J. Heidepriem, V. Krähling, C. Dahlke, T. Wolf, F. Klein, M. M. Addo, S. Becker, F. F. Loeffler, *Biotechnol. J.* **2020**, 15, 2000069.
- [35] P. Becquart, T. Mahlaköiv, D. Nkoghe, E. M. Leroy, *PLoS One* **2014**, 9, e96360.
- [36] L. Fabbri, *J. Org. Chem.* **2020**, 85, 12212.

- [37] Y. Jia, J. Li, *Chem. Rev.* **2015**, *115*, 1597.
- [38] A. L. Berhanu, Gaurav, I. M. , A. K. Malik, J. S. Aulakh, V. Kumar, K. Kim, *Trends Anal. Chem.* **2019**, *116*, 74.
- [39] V. S. Padalkar, S. Seki, *Chem. Soc. Rev.* **2016**, *45*, 169.
- [40] A. A. Nagarkar, S. E. Root, M. J. Fink, A. S. Ten, B. J. Cafferty, D. S. Richardson, M. Mrksich, G. M. Whitesides, *ACS Cent. Sci.* **2021**, *7*, 1728.
- [41] M. Mende, A. Tsouka, J. Heidepriem, G. Paris, D. S. Mattes, S. Eickelmann, V. Bordoni, R. Wawrzinek, F. F. Fuchsberger, P. H. Seeberger, C. Rademacher, M. Delbianco, A. Mallagaray, F. F. Loeffler, *Chem. - Eur. J.* **2020**, *26*, 9655.
- [42] J. Zhang, Y. Liu, S. Ronneberger, N. V. Tarakina, N. Merbouh, F. F. Loeffler, *Adv. Mater.* **2022**, *34*, 2108493.
- [43] G. Paris, J. Heidepriem, A. Tsouka, M. Mende, S. Eickelmann, F. F. Loeffler, in *SPIE BiOS 2019*, SPIE, San Francisco **2019**.
- [44] G. Paris Python scripts, available on github: App.py, laserClient.py, robot.py, and SAT in Spots we Trust.py, <https://github.com/Grigori-Paris/Grigori-Paris-PhD-code> (accessed: April 2021).
- [45] C. A. Schneider, W. S. Rasband, K. W. Eliceiri, *Nat. Methods* **2012**, *9*, 671.
- [46] G. Paris Python scripts, available on github: HoughCircleSynthesis.py and HoughCircleSynthesisApp.py, <https://github.com/Grigori-Paris/Grigori-Paris-PhD-code> (accessed: March 2021).
- [47] J. Danglad-Flores, S. Eickelmann, H. Riegler, *Chem. Eng. Sci.* **2018**, *179*, 257.
- [48] J. Danglad-Flores, S. Eickelmann, H. Riegler, *Eng. Rep.* **2021**, *3*, e12390.
- [49] C. P. Gordon, *Org. Biomol. Chem.* **2018**, *16*, 180.
- [50] T. Wolf, G. Kann, S. Becker, C. Stephan, H. R. Brodt, P. de Leuw, T. Grunewald, T. Vogl, V. A. Kempf, O. T. Keppler, K. Zacharowski, *Lancet* **2015**, *385*, 1428.